Murine ultrasound imaging for circumferential strain analyses in the angiotensin II abdominal aortic aneurysm model

John T. Favreau, BS,[a,b] Binh T. Nguyen, MD,[b] Ian Gao, BS,[b] Peng Yu, MD,[b] Ming Tao, MD,[b] Jacob Schneiderman, MD,[b] Glenn R. Gaudette, PhD,[a] and C. Keith Ozaki, MD,[b] *Worcester and Boston, Mass*

Objective: **The underlying causes of abdominal aortic aneurysms (AAAs) remain obscure, although research tools such as the angiotensin II (Ang II) apolipoprotein E-deficient (apoE$^{-/-}$) mouse model have aided investigations. Longitudinal imaging and determination of biomechanical forces in this small-scale model have been difficult. We hypothesized that high-frequency ultrasound biomicroscopy combined with speckle-tracking analytical strategies can be used to define the role of circumferential mechanical strain in AAA formation in the Ang II/apoE$^{-/-}$ mouse model of AAAs. We simultaneously examined dietary perturbations that might impact the biomechanical properties of the aortic wall, hypothesizing that the generalized inflammatory phenotype associated with diet-induced obesity would be associated with accelerated loss of circumferential strain and aneurysmal aortic degeneration.**

Methods: **Receiving either a 60 kcal% fat Western diet or standard 10 kcal% fat normal chow, Ang II-treated apoE$^{-/-}$ mice (n = 34) underwent sequential aortic duplex ultrasound scan imaging (Vevo 2100 System; VisualSonics, Toronto, Ontario, Canada) of their entire aorta. Circumferential strains were calculated using speckle-tracking algorithms and a custom MatLab analysis.**

Results: **Decreased strains in all aortic locations after just 3 days of Ang II treatment were observed, and this effect progressed during the 4-week observation period. Anatomic segments along the aorta impacted wall strain (baseline highest in ascending aorta; $P < .05$), whereas diet did not. At 2 and 4 weeks, there was the largest progressive decrease in strain in the paravisceral/supraceliac aorta ($P < .05$), which was the segment most likely to be involved in aneurysm formation in this model.**

Conclusions: **In the Ang II/apoE$^{-/-}$ aneurysm model, the aorta significantly stiffens (with decreased strain) shortly after Ang II infusion, and this progressively continues through the next 4 weeks. High-fat feeding did not have an impact on wall strain. Delineation of biomechanical factors and AAA morphology via duplex scan and speckle-tracking algorithms in mouse models should accelerate insights into human AAAs. (J Vasc Surg 2012;56:462-9.)**

Clinical Relevance: **Aortic aneurysms continue to cause substantial morbidity and mortality, although causes of aneurysms remain obscure. The current work combines a commonly used mouse model of aortic aneurysms, sophisticated ultrasonography, and special mathematical analyses to improve the utility of these tools for dissection of the mechanisms of aortic aneurysmal degeneration.**

Despite knowledge insights over the last decades, the molecular mechanisms of aortic aneurysmal disease remain obscure. Beyond some known clinical risk factors, biomechanical forces contribute to abdominal aortic aneurysm (AAA) development, progression, and rupture.[1-3] The composition and mechanical properties of AAAs are different from those of normal aortas,[4] with AAAs being stiffer and less distensible than nonaneurysmal aortas.

Murine models have emerged as a tool to enhance understanding of aneurysms,[5,6] although biomechanical studies have been limited in these models. One of the most commonly used models involves subcutaneous delivery of angiotensin II (Ang II) into apolipoprotein E-deficient (apoE$^{-/-}$) mice via an implanted osmotic pump.[5,7-10] Despite widespread clinical value, the use of longitudinal imaging in these aneurysm models remains scarce and underutilized because the small size of the animals makes the quantification and characterization of AAA progression difficult and time-consuming. Current methods for measuring aneurysm biomechanics and progression are simplistic in that they assess only the gross appearance of the aorta,[11] the maximum diameter of the aorta in situ,[12] or the luminal diameter ex vivo.[13] To date, a few in vivo imaging studies have been done on small animal AAA models, but they also only measured aortic diameters.[14-17] Recently, high-frequency ultrasound imaging systems (eg, Vevo 2100; VisualSonics, Toronto, Ontario, Canada) have been

From the Department of Biomedical Engineering, Worcester Polytechnic Institute, Worcester[a]; and the Division of Vascular and Endovascular Surgery, Brigham and Women's Hospital/Harvard Medical School, Boston.[b]

The study was funded by the National Heart, Lung, and Blood Institute R01HL079135, 1R01HL079135-06S1, T32HL007734; and the Carl and Ruth Shapiro Family Foundation.

Author conflict of interest: none.

Reprint requests: C. Keith Ozaki, MD, Brigham and Women's Hospital, Division of Vascular and Endovascular Surgery, Harvard Medical School, 75 Francis Street, Boston, MA 02115 (e-mail: ckozaki@partners.org).

The editors and reviewers of this article have no relevant financial relationships to disclose per the JVS policy that requires reviewers to decline review of any manuscript for which they may have a conflict of interest.

0741-5214/$36.00

doi:10.1016/j.jvs.2012.01.056

Table. Experimental groups and numbers of animals

Diet	*Age at implant*	*Ultrasound scan acquisition*
Normal chow (10 kcal% fat)	16 weeks	Pre-op, day 3 (n = 8); pre-op, day 14, day 28 (n = 10)
High fat (60 kcal% fat)	16 weeks	Pre-op, day 3 (n = 6); pre-op, day 14, day 28 (n = 10)

Pre-op, Preoperative.

developed to noninvasively microimage mice in vivo, and such approaches can reliably detect and measure the luminal diameter of AAA in apoE$^{-/-}$ mice infused with Ang II.[14,18] At the same time, speckle-tracking technology in ultrasound imaging has emerged as a quantitative, objective technique to accurately evaluate myocardial function and dynamics. Speckle tracking functions by tracing the displacement of speckles during the cardiac cycle to measure strain and strain rate,[19-22] and it has been used in the assessment of mouse models of cardiac dysfunction.[23]

Therefore, we hypothesized that high-frequency ultrasound scan biomicroscopy combined with speckle-tracking analytical strategies can be used to define the role of circumferential mechanical strain in AAA formation in defined aortic anatomic regions in the Ang II/apoE$^{-/-}$ mouse model of AAAs, with Ang II decreasing strain even preceding aneurysm development in defined anatomic locations. We simultaneously examined dietary perturbations that might impact the biomechanical properties of the aortic wall in these mice, hypothesizing that the generalized inflammatory phenotype associated with diet-induced obesity would be associated with accelerated loss of circumferential strain and aneurysmal aortic degeneration.

METHODS

Animals and angiotensin II mini-pump insertion. Male apoE-deficient mice (B6.129P2-Apoe^{tm1Unc}/J) were purchased from the Jackson Laboratory (Bar Harbor, Me) and maintained on a 12-hour light-dark cycle and received water and assigned chow ad libitum. All animal experiments were performed according to protocols approved by the Institutional Animal Care and Use Committee and complied with the Guide for the Care and Use of Laboratory Animals (National Institutes of Health Publication No. 85-23, Revised 1996).

At 16 weeks of age, osmotic mini-pumps (Model 1002; Alzet Scientific Products, Cupertino, Calif) loaded with Ang II (500-1000 ng/min/kg) were sterilely implanted in the dorsal subcutaneous tissues under 1% to 2% isoflurane inhalant anesthesia with oxygen at 1 L/minute, and wounds were closed with absorbable sutures.

Dietary perturbations. All animals received a 10 kcal% fat standard chow diet after weaning (D12450B; Research Diets, New Brunswick, NJ). The normal chow group was maintained on this diet throughout the course of the experiment. To study the effect of diet-induced obesity on aortic wall elasticity, animals designated as high fat were prefed with a 60 kcal% fat Western diet (D12492; Research Diets) 6 weeks before Ang II infusion and maintained on this diet during the study. The Table summarizes the experimental groups and the specific diets over time.

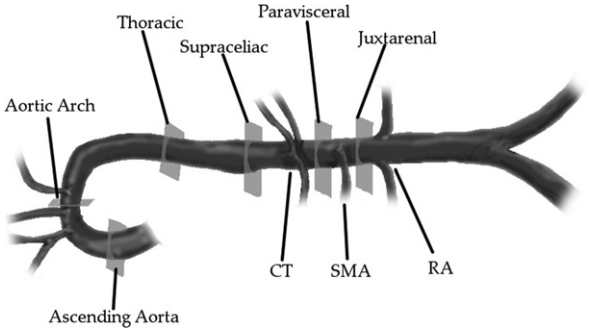

Fig 1. Segments of interest analyzed in the thoracic and abdominal aorta. Celiac trunk (*CT*), superior mesenteric artery (*SMA*), and renal arteries (*RAs*). The thoracic region = cross-section 5 mm proximal to the CT; the supraceliac region = cross-section 1 mm proximal to the CT; the paravisceral region = cross-section between the CT and SMA; and the juxtarenal region = cross-section 1 mm distal to the SMA.

Ultrasound imaging. High-resolution ultrasonography was performed using a Vevo 2100 Imaging System with MS700 (30-70 MHz) and MS550D (22-55 MHz) linear array transducers (VisualSonics). For short-term study groups, data were collected before implantation (preoperatively) and at day 3 after implantation, whereas for long-term groups, data were collected preoperatively, at day 14, and at day 28 after implantation. Mice were anesthetized using 1% to 2% isoflurane inhalant anesthesia with oxygen at 1 L/minute and animals were placed in the supine position on a moveable, heated stage maintained at 37°C. Hair was removed from the abdomen and thorax using a depilatory cream. Warmed ultrasound scan transmission gel was applied to the ventral surface of the animal and the probe was positioned on a fixed stand perpendicular to the stage. After adequate visualization of the aortic segments of interest, 100-frame (at 240-270 frames/second) B-mode cine image sequences were then recorded over an average of two to three cardiac cycles. Because aortic pathologies associated with Ang II infusion frequently occur at defined locations along the aorta (arch and suprarenal > infrarenal and thoracic), six different anatomic segments were chosen to allow for comparisons of mechanical strains at these locations (Fig 1).

Ultrasound data analysis. Ultrasound scan cine loops collected during the imaging procedure were analyzed to calculate circumferential strains. Cine loops were loaded into VevoStrain 2100 Advanced Cardiac Analysis

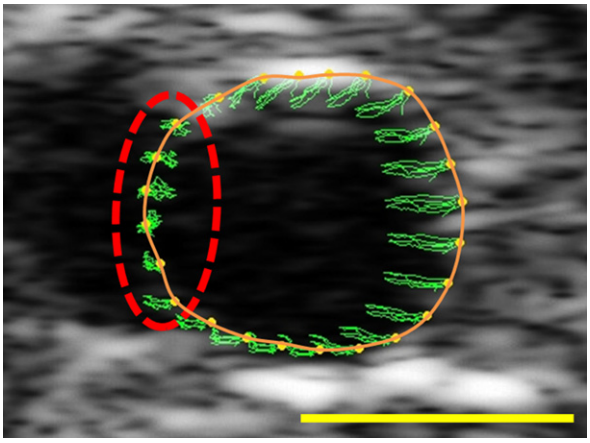

Fig 2. Sample ultrasound scan image of an aorta, with the manually drawn spline shown (*solid orange*). *Green traces* show the path of the tracking points (*yellow*) throughout several cardiac cycles. The *dashed red line* indicates a region that has poor contrast (likely due to a branching vessel) and therefore poor tracking. These regions were dropped from the analyses to improve accuracy. *Yellow scale bar* = 1 mm.

Software (VisualSonics) and analyzed using the manufacturer's cardiac speckle-tracking algorithm. A closed spline of 48 points was manually drawn around the intraluminal edge of the vessel cross-section in the ultrasound image. Accuracy of speckle-tracking throughout the cine loop was verified visually. To accomplish this, the vessel wall was traced on the first frame of the cine loop. The ultrasound cine loop was then viewed and it was ensured that the tracing closely followed the movement of the vessel wall throughout each cardiac cycle. If tracking did not pass visual inspection, the splines were redrawn until adequate tracking was achieved. The frame-to-frame displacements of each of the 48 points throughout the cine loop were the output for strain analysis. Additionally, representative frames from the ultrasound images were saved to allow determination of vessel regions that did not have enough speckle contrast for adequate analysis (regions that correspond to renal artery branching or echogenic shadow artifacts; Fig 2).

Displacements from the VevoStrain software were then imported into a custom MatLab program (Mathworks, Natick, Mass) and analyzed to determine circumferential strain from displacements. Strains were determined at each of the 48 points around the vessel. Circumferential strains were calculated using the definition of the Cauchy strain tensor for cylindrical coordinates.[24] Radii were measured by determining the distance from each point to the centroid of the points around the vessel. It was assumed that the local radius around each measured point was constant at any particular time point. The strains at each point around the vessel were averaged to give a mean incremental strain from frame to frame. The analysis points were then compared with images from the ultrasound machine. Regions that appeared dark and which had no speckle contrast were then manually dropped from the analysis. An example of these regions is shown with a dashed red line in Fig 2. After excluding such uninterpretable regions, average strain curves were plotted, and peaks and troughs were located and manually verified using a custom MatLab program (Mathworks). The maximum circumferential strain value was calculated as the average difference between consecutive peaks to troughs throughout each cine loop. Resulting means were then averaged in each experimental group at each aortic location and reported as mean ± SEM. In addition to calculating strains, vessel cross-sectional areas were determined from scaled ultrasound images. These areas were then used to determine if vessel diameters changed throughout the study.

Statistical analyses. Statistical analyses were executed using Sigmaplot 11 (SYSTAT Software, San Jose, Calif). Comparisons between the two groups were completed using an unpaired two-tailed *t*-test. Comparisons between three or more experimental groups and between time points were made using one-way analysis of variance (ANOVA) with Tukey post-hoc analyses. All data are reported as mean ± SEM.

RESULTS

Effect of high-fat diet on mechanical strain. The normal chow and high-fat mice gained weight as expected based on vendor-supplied data (Jackson Laboratory). To confirm the ability to measure strain in the mouse aorta, preoperative baseline data for mice in the four study groups were analyzed. Data from all normal chow diet mice with all high-fat diet mice were compared first (Fig 3). The results demonstrate a consistency of measurements in the same aortic location with animals consuming the same diet. Additionally, our strain values were similar (maximum strains ~19% to 20%) to those reported by Goergen et al[25] using magnetic resonance imaging. It also shows no statistically significant differences between normal chow and high-fat diet mice at each segment along the aorta preoperatively. However, differences in mechanical strain along the aorta in the normal chow and high-fat groups were noted. The major trend seen here is that in both the normal chow and high-fat groups, the ascending aorta shows statistically significant higher strain values than the other anatomical locations ($P < .05$). Additionally, the lowest strain values were observed in the arch segment ($P < .05$).

Short-term impact of angiotensin II treatment on mechanical strain. Using the short-term arm of the study, the acute effects of the Ang II treatment (1000 ng/kg/min) on mechanical strain in normal chow and high-fat mice (Fig 4, *A*) were isolated. There is a consistent trend toward decreased strains in all aortic locations after just 3 days of Ang II treatment in the normal chow group. Reductions in the supraceliac, thoracic, and ascending aortic locations were statistically significant ($P < .05$). None of these animals showed changes in aortic diameter at day 3 post-Ang II infusion.

Similar results were found in the short-term study for the mice fed a high-fat diet (Fig 4, *B*). In this group, there

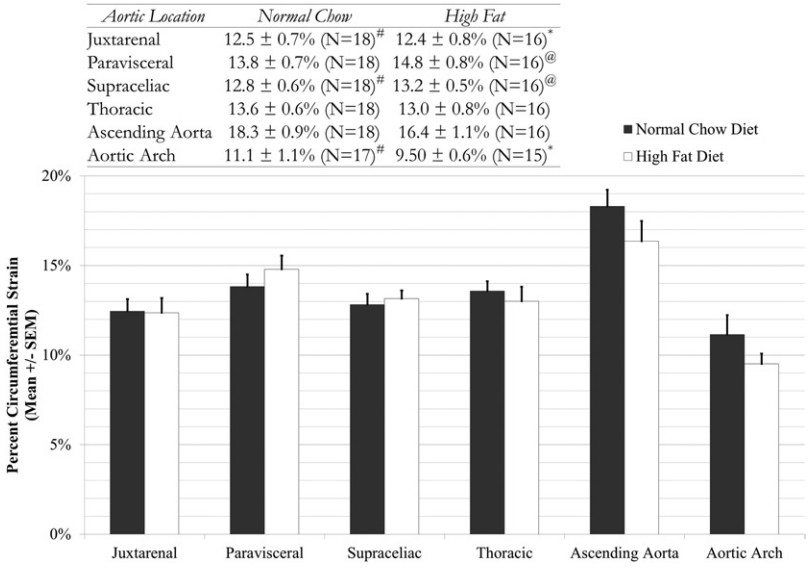

Fig 3. Comparison of baseline preoperative strain magnitudes across six aortic locations between normal chow and high-fat diet mice. Statistical statements are noted in the inset table. No statistically significant differences were found between mice of different diets in any aortic location, although differentials were noted among segments as depicted. All statistical statements indicate that $P < .05$; all groups contain 15 or more animals. *Indicates statistical difference from high-fat ascending aorta; #indicates statistical difference from normal chow ascending aorta; and @indicates statistical difference from high-fat aortic arch.

was a similar trend toward decreased strain at the day 3 time point, with statistically significant decreases occurring in the supraceliac segment. Unlike the normal chow group, however, two animals in this group formed aortic aneurysms (at least 1.5 times greater diameter than initial measurement) by day 3 postoperatively, while one animal died of an aortic arch rupture before day 3. Aneurysms formed in these animals were found in the paravisceral and supraceliac regions.

Long-term effects of angiotensin II treatment on mechanical strain. Long-term changes in strain were analyzed for both the normal chow and high-fat groups receiving Ang II (500 ng/kg/min). In both groups, there was a progressive trend toward decreased mechanical strains from preoperative to day 14 to 28 strains (Fig 4, *C* and *D*). The largest reduction of strain was observed in the paravisceral and the supraceliac segments in high-fat diet mice (Fig 4, *D*). The majority of these reductions in strain corresponded directly with aneurysm formation. It should be noted that both the normal chow and high-fat groups contained animals with and without aneurysm development by day 28.

Relative effects of different factors on mechanical strain. The design of this study enabled the isolation of the effects of Ang II treatment from those of aneurysm formation. The percent change in strain from the preoperative strain due to Ang II treatment alone, aneurysm formation at day 14, and aneurysm formation at day 28 for normal chow and high-fat animals was determined (Fig 5). These data suggest that both the Ang II treatment and the actual formation of aneurysm play a role in reducing strain in the aorta. The results in Fig 5 also suggest that aneurysmal degeneration and physical remodeling of the wall may play a large role in decreasing circumferential strains. Mural thrombus was a common finding in the Ang II mice. The thrombus likely contributed to the overall decrease in strain of the aneurysmal aortic wall. However, the current study does not have enough power to tease out the component contributions of mural thrombus vs other factors on the decreased strain found in aneurysmal segments.

Overall, in this study, there were clear differences in aneurysm formation between the normal chow and high-fat diet groups. At day 3 in the short-term arm of our study, 0% (n = 8) of normal chow animals had formed aneurysms. High-fat animals at day 3, however, demonstrated an aneurysm formation rate of 50% (n = 6). One of these high-fat animals died of aortic arch aneurysm and rupture before day 3. In the long-term arm, similar rates of aneurysm formation between normal chow and high-fat animals were observed. At week 4, there was an aneurysm rate of 70% (including animals which died of aneurysmal arch rupture by week 4). In contrast, an aneurysm formation rate of 88% was seen in high-fat animals. We were not, however, able to distinguish a difference in pre-Ang II strain measurements in animals that subsequently developed aneurysms vs no aneurysms (no predictive capability).

DISCUSSION

AAAs lead to over 15,000 deaths per year in the United States alone, and some even estimate the annual death rate

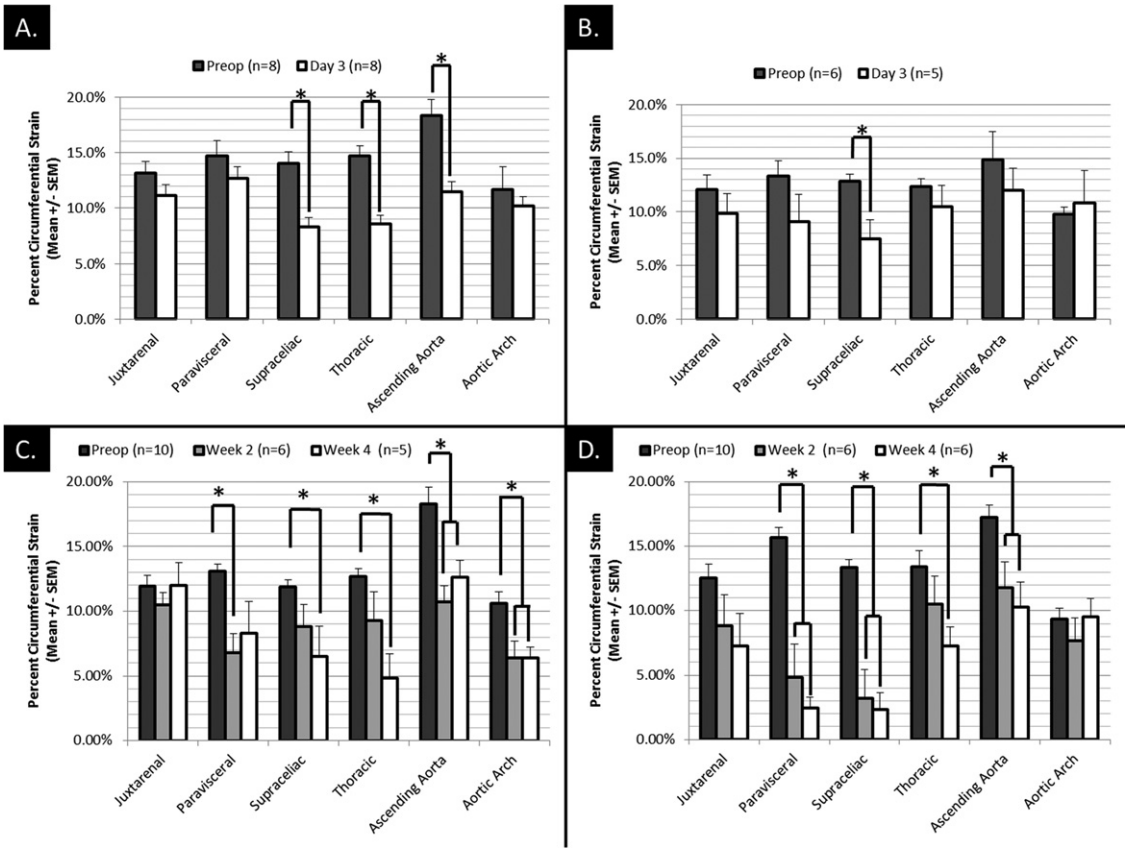

Fig 4. **A**, Short-term effects of angiotensin II (Ang II) treatment on animals fed on normal chow diets. **B**, Short-term effects of Ang II treatment on animals consuming only high-fat diets since week 10 of age. **C**, Long-term effects of Ang II treatment on normal chow animals. **D**, Long-term effects of Ang II on high-fat animals. *Indicates $P < .05$.

from AAAs to be as high as 30,000. Most patients are asymptomatic until catastrophic rupture, and ruptured AAAs continue to have high morbidity and mortality.[26] Hence, there is an undeniable need to fully understand the pathophysiology of AAAs and to improve patient selection for expansion and rupture prediction and prevention.

The exact pathogenesis of AAAs is complex and still unknown, but clinical risk factors are known: smoking, male gender, age, family history, previous vascular disease, hypertension, and hypercholesterolemia.[6] Biologically, aortic wall inflammation and oxidative stress seem to hold a role in AAA formation.[27] The immune system is also believed to be mechanistically involved in the development of AAAs, along with a reduction in the density of smooth muscle cells, elastin, and collagen fibers, which are degraded by proteolytic enzymes (mostly matrix metalloproteinases).[28] The aortic wall structurally depends on elastin and collagen, but in aneurysm disease, medial elastin degradation (elastolysis) occurs causing dilatation of the aorta.[6]

Biomechanical forces stand as a pivotal factor in AAA development and rupture.[1-3,29] Peak AAA wall stress may be superior to maximum diameter in differentiating rupture risk.[1,3] Additionally, due to unevenly distributed wall stresses, overall, AAA wall stress does not directly depend on maximum diameter.[30]

Ultrasound scan serves as a useful tool not only clinically for infrarenal aortic aneurysm surveillance but also experimentally for quantification of aortic morphology and biomechanics. Contemporary high-frequency ultrasound scan represents a significant improvement over prior techniques in evaluating the aorta in murine AAA models. The approach is relatively noninvasive imaging, can be performed longitudinally, allows for examination of aneurysm-prone/protected regions, and in combination with analytical approaches, such as speckle tracking for strain analyses, it provides more information than previous murine AAA imaging studies that only measured maximum aortic diameter. The primary downside is the expense of the device and technical expertise needed to acquire image data, although it has been shown that high-frequency ultrasound scan can be performed with relatively small intraindividual and interindividual variance.[14] Other groups have used in vivo pulse wave velocity in nonaneurysm studies to show that apoE$^{-/-}$ mice infused with Ang II have significantly increased vessel stiffness compared with controls after 30 days.[31] However, this report did not provide localized

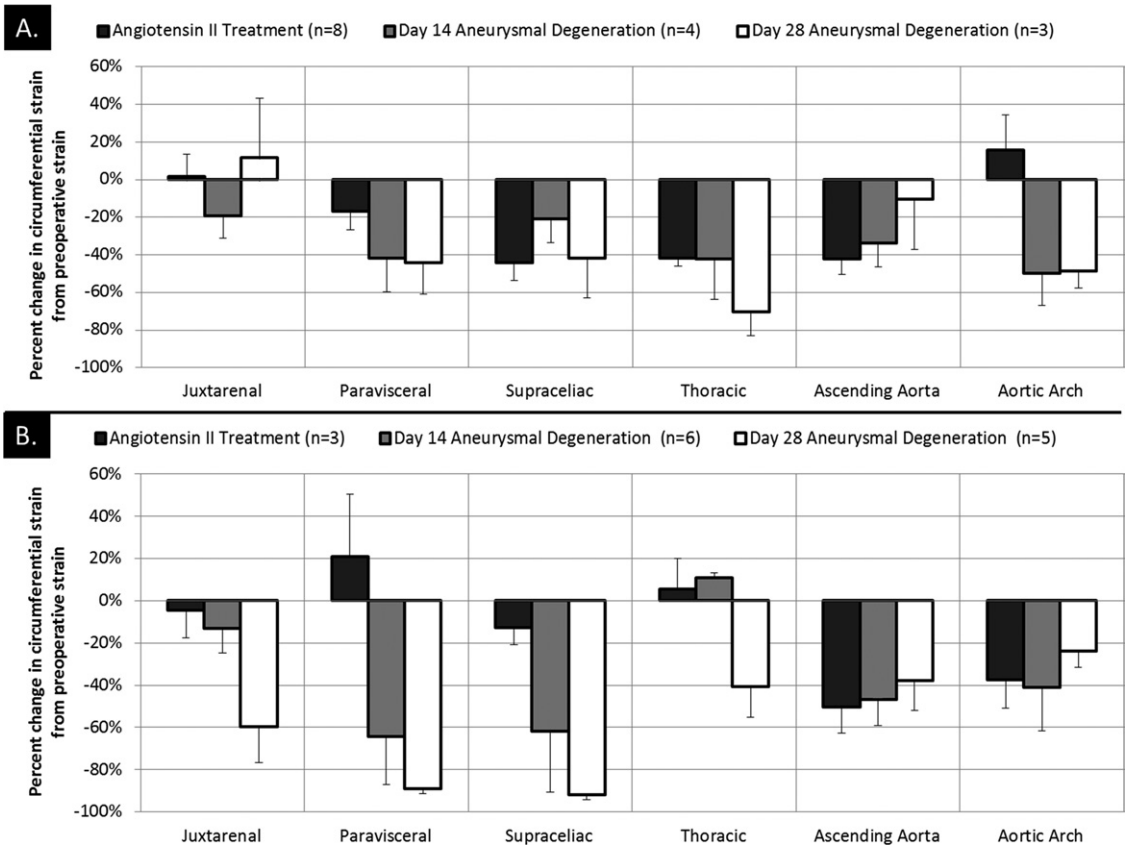

Fig 5. Effects of angiotensin II (Ang II) and aneurysmal degeneration on aortic wall strain. Data are reported as percent change in strain from preoperative strain. The Ang II group contains only animals that did not have aneurysms at day 3 from the early study. Day 14 and day 28 aneurysmal degeneration groups only contain data from animals that had aneurysmal expansion (increase in size of 150% or more) detected via ultrasound scans. Data for normal chow and high-fat groups are shown in **(A)** and **(B)**, respectively.

stiffness data. Other related imaging modalities are in development for in vivo murine studies, for example, quantification of murine aortic cyclic strain and motion using three-dimensional magnetic resonance angiography in relation to its implications for AAA growth.[25]

In the current experiment, high-frequency ultrasound scan was used to assess aortic wall strain in apoE$^{-/-}$ mice at selected time points during Ang II-induced aortic aneurysm development. Wall strain correlated with the pathologic events that occurred in different segments of the aorta. Baseline wall strain was measured in selected segments along the aorta, revealing a rather high strain in the ascending aorta, while the aortic arch manifested the lowest basic strain. As Ang II was given to our mice, the ascending segment did not manifest aneurysmal dilatation. However, as expected, the arch responded dramatically by developing aneurysms, some of which ruptured within the very early stage (3 days). Cao et al[9] described the phenomenon of early development of aneurysm with subsequent rupture, ranging at 25% of all mice. In their series, 44% of patients presented with arch aneurysms. The prevalence of early development of aortic aneurysm correlates with age. Also, it is assumed to represent a genetic predilection of some of the apoE$^{-/-}$ mice, presenting with aortic arch structural aberration, which yields a stiffer vessel wall. The later phase of Ang II infusion (as assessed on days 14 through 28) was characterized by a significant reduction of wall strain in the suprarenal segment, namely the paravisceral and supraceliac regions. It is not surprising therefore that those segments are most affected by aneurysm formation in this model. Notably, the aneurysmal dilatation by itself leads to an increased vessel diameter, which further decreases wall strain locally. The data collected via longitudinal noninvasive assessments emphasize the significance of anatomical localization of regional circumferential wall strain characteristics as a predictor for potential future events.

Dietary manipulations of murine models have emerged as a useful experimental tool,[32] and such manipulations are known to impact factors key to development of arterial aneurysms.[33] Obesity has been shown to increase periaortic adipose tissue inflammation leading to enhanced incidence of AAAs in the Ang II murine model. We sought to characterize the effect of these changes on the aortic wall elasticity and association with enhanced aneurysm forma-

tion. Under the conditions of our experiments, we found no differences between normal chow mice and high-fat mice in any region along the aorta preoperatively. This suggests that the hyperlipidemic state associated with short-term high-fat feeding alone does not significantly alter the structural components of the aortic wall, but rather it enhances the inflammatory and remodeling response associated with Ang II treatment. There was no significant difference between atherosclerotic plaque deposition on the aortic wall observed at autopsy between the normal chow and high-fat animals. However, longer-term high-fat feeding as well as more advanced age may lead to enhanced atherosclerotic changes that can result in loss of aortic elasticity and increased risk for aneurysmal degeneration, but this remains to be characterized in future investigations.

Potential parallel applications for high-frequency ultrasound scans are numerous. Our methods could be used to quantify circumferential strain in other murine models of disease and after interventions (eg, statins, antihypertensive therapies, anti-inflammatory agents). Furthermore, most AAAs are asymmetric. It has been shown that asymmetry/shape has a substantial influence on the distribution of wall stress within the aneurysm,[1] and our strategies could be expanded to interrogate the effect of asymmetric circumferential strain on AAA formation and rupture. Finally, clinically there are significant shortfalls with current AAA management pathways, as the fundamental strategy of using size imaging as a stand-alone to diagnose and provide prognostic information regarding AAAs does not provide complete data to identify which AAAs are most likely to continue to increase in size and be at risk for rupture. A more complete ability to predict AAA progression may allow improved AAA management.[34]

A limitation of this study was that blood pressure was not closely measured in the mice. However, it has been reported previously that blood pressure does not affect Ang II-related AAA development,[35] and it is likely that for the range of blood pressures for the experimental animals, the impact on strain is minimal. Systemic blood pressure is necessary for calculation of stiffness index and other relevant hemodynamic parameters. We assumed that at day 3, no animals would develop gross aneurysmal changes and that any difference in strain measured would be from the effect of Ang II alone rather than contributions from structural changes from an enlarging aneurysm/thrombus. The combination of high-fat feeding and high Ang II dose led to unexpected aneurysm development at day 3. It is possible that by reducing the dose of Ang II, we could decrease the rate of early aneurysm formation and better determine the effects of the Ang II treatment alone. Finally, due to the resolution limitations of current ultrasound scan technology, we were unable to accurately differentiate between the intraluminal and extraluminal aortic wall. For these reasons, we only calculated and reported the circumferential strains (not radial strain) on the intraluminal wall, which was clearly visible in the ultrasound images.

In conclusion, the combination of high-frequency ultrasound imaging and speckle tracking allows the quantification of the changes in circumferential strain of the aorta during AAA development in apoE$^{-/-}$ mice infused with Ang II. The combination of these techniques demonstrated that the aorta significantly stiffens (has decreased strain) shortly after the infusion of Ang II into apoE$^{-/-}$ mice and after aneurysm formation in these mice. Measurements at later time points revealed progressive decrease in strain in the suprarenal aorta, which is the segment most likely to be involved in aneurysm formation. The delineation of the biomechanical factors and natural history of AAA development in animal models of the disease in combination with our continuously improving armamentarium of biologic assays will provide insights into the factors associated with initiation and propagation of AAAs in humans.

AUTHOR CONTRIBUTIONS

Conception and design: JF,BN,GG,CO
Analysis and interpretation: JF, BN, IG, JS, GG, CO
Data collection: JF, BN, IG, PY, MT
Writing the article: JF, BN, IG, PY, JS, GG, CO
Critical revision of the article: JF, BN, IG, PY, MT, JS, GG, CO
Final approval of the article: JF, BN, IG, PY, MT, JS, GG, CO
Statistical analysis: JF, BN, IG
Obtained funding: CO, GG, JS, BN
Overall responsibility: CO
JF and BN contributed equally to this article.

REFERENCES

1. Vorp DA, Raghavan ML, Webster MW. Mechanical wall stress in abdominal aortic aneurysm: influence of diameter and asymmetry. J Vasc Surg 1998;27:632-9.
2. Vorp DA. Biomechanics of abdominal aortic aneurysm. J Biomech 2007;40:1887-902.
3. Fillinger MF, Marra SP, Raghavan ML, Kennedy FE. Prediction of rupture risk in abdominal aortic aneurysm during observation: wall stress versus diameter. J Vasc Surg 2003;37:724-32.
4. He CM, Roach MR. The composition and mechanical properties of abdominal aortic aneurysms. J Vasc Surg 1994;20:6-13.
5. Daugherty A, Cassis LA. Mouse models of abdominal aortic aneurysms. Arterioscler Thromb Vasc Biol 2004;24:429-34.
6. Thompson RW. Basic science of abdominal aortic aneurysms: emerging therapeutic strategies for an unresolved clinical problem. Curr Opin Cardiol 1996;11:504-18.
7. Daugherty A, Manning MW, Cassis LA. Angiotensin II promotes atherosclerotic lesions and aneurysms in apolipoprotein E-deficient mice. J Clin Invest 2000;105:1605-12.
8. Wang YX, Martin-McNulty B, Freay AD, Sukovich DA, Halks-Miller M, Li WW, et al. Angiotensin II increases urokinase-type plasminogen activator expression and induces aneurysm in the abdominal aorta of apolipoprotein E-deficient mice. Am J Pathol 2001;159:1455-64.
9. Cao RY, Amand T, Ford MD, Piomelli U, Funk CD. The murine angiotensin II-induced abdominal aortic aneurysm model: rupture risk and inflammatory progression patterns. Front Pharmacol 2010;1:9.
10. Manning MW, Cassi LA, Huang J, Szilvassy SJ, Daugherty A. Abdominal aortic aneurysms: fresh insights from a novel animal model of the disease. Vasc Med 2002;7:45-54.

11. Daugherty A, Manning MW, Cassis LA. Antagonism of AT2 receptors augments angiotensin II-induced abdominal aortic aneurysms and atherosclerosis. Br J Pharmacol 2001;134:865-70.
12. Bergoeing MP, Arif B, Hackmann AE, Ennis TL, Thompson RW, Curci JA. Cigarette smoking increases aortic dilatation without affecting matrix metalloproteinase-9 and −12 expression in a modified mouse model of aneurysm formation. J Vasc Surg 2007;45:1217-27.
13. Sho E, Sho M, Nanjo H, Kawamura K, Masuda H, Dalman RL. Hemodynamic regulation of $CD34^+$ cell localization and differentiation in experimental aneurysms. Arterioscler Thromb Vasc Biol 2004; 24:1916-21.
14. Barisione C, Charnigo R, Howatt DA, Moorleghen JJ, Rateri DL, Daugherty A. Rapid dilation of the abdominal aorta during infusion of angiotensin II detected by noninvasive high-frequency ultrasonography. J Vasc Surg 2006;44:372-6.
15. Chiou AC, Chiu B, Oppat WF, Matsumura JS, Chisholm RL, Pearce WH. Transrectal ultrasound assessment of murine aorta and iliac arteries. J Surg Res 2000;88:193-9.
16. Knipp BS, Ailawadi G, Sullivan VV, Roelofs KJ, Henke PK, Stanley JC, et al. Ultrasound measurement of aortic diameters in rodent models of aneurysm disease. J Surg Res 2003;112:97-101.
17. McFadden EP, Chaabane L, Contard F, Guerrier D, Briguet A, Douek P, et al. In vivo magnetic resonance imaging of large spontaneous aortic aneurysms in old apolipoprotein E-deficient mice. Invest Radiol 2004; 39:585-90.
18. Martin-McNulty B, Vincelette J, Vergona R, Sullivan ME, Wang YX. Noninvasive measurement of abdominal aortic aneurysms in intact mice by a high-frequency ultrasound imaging system. Ultrasound Med Biol 2005;31:745-9.
19. Bauer M, Cheng S, Jain M, Ngoy S, Theodoropoulos C, Trujillo A, et al. Echocardiographic speckle-tracking based strain imaging for rapid cardiovascular phenotyping in mice. Circ Res 2011;108:908-16.
20. Mondillo S, Galderisi M, Mele D, Cameli M, Lomoriello VS, Zacà V, et al. Speckle-tracking echocardiography: a new technique for assessing myocardial function. J Ultrasound Med 2011;30:71-83.
21. Dandel M, Hetzer R. Echocardiographic strain and strain rate imaging—clinical applications. Int J Cardiol 2009;132:11-24.
22. Leung DY, Ng AC. Emerging clinical role of strain imaging in echocardiography. Heart Lung Circ 2010;19:161-74.
23. Peng Y, Popovic ZB, Sopko N, Drinko J, Zhang Z, Thomas JD, et al. Speckle tracking echocardiography in the assessment of mouse models of cardiac dysfunction. Am J Physiol Heart Circ Physiol 2009; 297:H811-20.
24. Fung YC. A first course in continuum mechanics. 3rd ed. Englewood Cliffs, NJ: Prentice Hall; 1993.
25. Goergen CJ, Barr KN, Huynh DT, Eastham-Anderson JR, Choi G, Hedehus M, et al. In vivo quantification of murine aortic cyclic strain, motion, and curvature: implications for abdominal aortic aneurysm growth. J Magn Reson Imaging 2010;32:847-58.
26. Roger VL, Go AS, Lloyd-Jones DM, Adams RJ, Berry JD, Brown TM, et al. Heart disease and stroke statistics—2011 update: a report from the American Heart Association. Circulation 2011;123:e18-e209.
27. Diehm N, Dick F, Schaffner T, Schmidli J, Kalka C, Di Santo S, et al. Novel insight into the pathobiology of abdominal aortic aneurysm and potential future treatment concepts. Prog Cardiovasc Dis 2007;50: 209-17.
28. Sakalihasan N, Limet R, Defawe OD. Abdominal aortic aneurysm. Lancet 2005;365:1577-89.
29. Steinman DA, Vorp DA, Ethier CR. Computational modeling of arterial biomechanics: insights into pathogenesis and treatment of vascular disease. J Vasc Surg 2003;37:1118-28.
30. McGloughlin TM, Doyle BJ. New approaches to abdominal aortic aneurysm rupture risk assessment: engineering insights with clinical gain. Arterioscler Thromb Vasc Biol 2010;30:1687-94.
31. Hartley CJ, Reddy AK, Madala S, Martin-McNulty B, Vergona R, Sullivan ME, et al. Hemodynamic changes in apolipoprotein E-knockout mice. Am J Physiol Heart Circ Physiol 2000;279:H2326-34.
32. Rossmeisl M, Rim JS, Koza RA, Kozak LP. Variation in type 2 diabetes—related traits in mouse strains susceptible to diet-induced obesity. Diabetes 2003;52:1958-66.
33. Police SB, Thatcher SE, Charnigo R, Daugherty A, Cassis LA. Obesity promotes inflammation in periaortic adipose tissue and angiotensin II-induced abdominal aortic aneurysm formation. Arterioscler Thromb Vasc Biol 2009;29:1458-64.
34. Moxon JV, Parr A, Emeto TI, Walker P, Norman PE, Golledge J. Diagnosis and monitoring of abdominal aortic aneurysm: current status and future prospects. Curr Probl Cardiol 2010;35:512-48.
35. Cassis LA, Gupte M, Thayer S, Zhang X, Charnigo R, Howatt DA, et al. ANG II infusion promotes abdominal aortic aneurysms independent of increased blood pressure in hypercholesterolemic mice. Am J Physiol Heart Circ Physiol 2009;296:H1660-5.

Submitted Dec 7, 2011; accepted Jan 23, 2012.